Arabian Journal for Science and Engineering (2018) 43:6305–6313
https://doi.org/10.1007/s13369-017-3013-1

RESEARCH ARTICLE - PETROLEUM ENGINEERING

A Model for Estimating the Saturation Exponent Based on NMR in Tight Sandy Conglomerate Reservoirs

Yan Kuang[1] · Liqiang Sima[1] · Zeyu Zhang[1] · Zhenlin Wang[2] · Meng Chen[3]

Received: 21 June 2017 / Accepted: 5 December 2017 / Published online: 18 December 2017

Abstract
The electrical resistivity of a porous medium, which is used for water or oil saturation evaluation through combination with Archie's law, strongly depends on the wettability and geometry of the pore system. In tight sandy conglomerate reservoirs, the pore-throat structure is so complicated that Archie's equation is non-applicable. Analysis shows that the saturation exponent n is a function of the water saturation (S_w), microstructure, and wettability. Here, a novel method based on nuclear magnetic resonance is proposed to determine the saturation exponent (n) under water- or oil-wet conditions. The Schlumberger Doll Research model is also introduced to estimate and analyze the fluid distribution in an irregular pore space. To validate the model, 21 water-wet core samples from the tight conglomerate reservoir in the Junggar Basin, Northwestern China, were selected to measure the electrical resistivity at varying water saturation levels. The absolute errors between the predicted and measured saturation exponents range from −0.153 to 0.131, and the absolute errors for the water saturation between the predicted and measured values vary from −0.032 to 0.023. These results indicate that the proposed model could be applied to accurately predict the water saturation in tight sandy conglomerate reservoirs.

Keywords Tight sandy conglomerate · Nuclear magnetic resonance · SDR model · Saturation exponent · Water-wet

1 Introduction

Electrical resistivity is one of the fundamental parameters required for estimating the water or oil saturation in reservoirs. The work of Archie [1] analyzed the experimental data of Gulf bay sandstones and proposed models to quantitatively evaluate the water saturation from the resistivity. The first equation defines the formation factor F as the ratio between the resistivity of a rock fully saturated with formation fluid R_o and the resistivity of the fluid itself R_w ($F = R_o/R_w = 1/\phi^m$), while the second equation defines the rock resistivity index RI as the ratio between the resistivity of the partially saturated rock R_t and R_o ($RI = R_t/R_o = 1/S_w^n$). The two equations can be integrated together as Eq. (1):

$$S_w^n = \frac{R_w}{\phi^m R_t} = \frac{F R_w}{R_t} \tag{1}$$

where m is the cementation exponent, which characterizes the pore shape interconnection, n is the saturation exponent, which is related to the pore fluid and pore geometry, ϕ is the porosity in fraction, S_w is the water saturation in fraction. Typically presented in the double logarithmic scale, m and n are the gradients of F–ϕ and RI–S_w, respectively.

However, further research shows that the F–ϕ and RI–S_w relationships were not always linear [2–4]. Examples of situation in which Archie's method would not work well are in shaly sandstones [5] and low permeability reservoirs [6] or situation where the method is influenced by excess clay conductivity [2,3], reservoir anisotropy [7,8], microporosity [9,10], grain shape [11], clay distribution [12], fluid distribution [13], and wettability [14,15]. Considering the various factors, Simandoux [16] studied "homogeneous mixtures of sorted sand and natural clay in various proportions" and proposed the Simandoux saturation equation. Poupon and Leveaux [17] proposed the "Indonesian" equation to cope

✉ Liqiang Sima
SSMML2016@qq.com

1 School of Geoscience and Technology, Southwest Petroleum University, Chengdu 610500, China

2 Research Institute of Exploration and Development, Xinjiang Oilfield Company, CNPC, Karamay 834000, People's Republic of China

3 State Key Laboratory of Oil and Gas Reservoir Geology and Exploitation, Southwest Petroleum University, Chengdu 610500, China

with the evaluation problems for certain clay-rich formations in Indonesia. The *Waxman–Smits* (W–S) saturation equation was developed from the recognition that cation exchange capacity measurements could be used to estimate and correct for the surface conductivity of clay minerals [18], which was then improved as the "dual-water" conductivity model by Clavier et al. [19]. Juhasz [20] used the density and neutron log data as a replacement for laboratory data and proposed another modification to the Waxman–Smits saturation equation. For the saturation exponent, Anderson [21] found that n, in particular, is extremely sensitive to wettability, and the effect was investigated by Man and Jing [15] based on a network model; the results showed that different wettability types give rise to different resistivity behaviors. Suman and Knight [14] also found that oil-wet systems display higher n values and hysteresis between the drainage and imbibition cycles. Kumar et al. [4] studied water-wet sandstones, and the results showed that n changes as a function of the confining pressure, microporosity, and saturation conditions.

All of the above examples illustrate the challenges associated with the determination of n. Given the importance of n in predicting hydrocarbon in place, we developed a model to predict n based on the equivalent channel model [22] in combination with the SDR model from NMR experiment data. The model was validated and applied to a tight sandy conglomerate reservoir in Junggar Basin, Northwestern China.

2 Theory

A porous media can be modeled as multi-curved capillary bundles [22], where F is related to the porosity (ϕ) and tortuosity (τ) of the pore network. These are related to the permeability k by the mean hydraulic radius r_{H}. This "equivalent channel model" can be further expanded:

$$F = \frac{\tau^2}{\phi} = \frac{r_{\mathrm{H}}^2}{bk} = \frac{(2V_{\mathrm{p}}/A_{\mathrm{p}})^2}{bk} \tag{2}$$

where V_{p} is the pore volume ($\mu\mathrm{m}^3$), A_{p} is the surface area of the pore interface ($\mu\mathrm{m}^2$), and b is a geometric factor.

According to the mechanism of NMR, in a uniform magnetic field with a short inter echo spacing where diffusion is ignored, the transversal relaxation time T_2 in a porous media is defined as [23]

$$\frac{1}{T_2} = \frac{1}{T_{2\mathrm{B}}} + \rho_2 \frac{A_{\mathrm{p}}}{V_{\mathrm{p}}} \tag{3}$$

where $T_{2\mathrm{B}}$ is the bulk transversal relaxation time of the fluid (ms), ρ_2 is the transverse surface relaxivity of the rock (μm/ms), and $A_{\mathrm{p}}/V_{\mathrm{p}}$ is the surface-to-volume ratio of the pore space ($\mu\mathrm{m}^{-1}$). Usually, we have $T_{2\mathrm{B}} \gg T_2$, so from Eq. (3), we can obtain

$$\frac{V_{\mathrm{p}}}{A_{\mathrm{p}}} = \rho_2 T_2 \tag{4}$$

The permeability k of porous media was estimated from the NMR correlation ϕ and T_1 as $k \sim \phi T_1^2$ in early works [24]. Then, this correlation was improved by Kenyon [25], with ϕT_1^2 replaced by $\phi^4 T_1^2$. During later research, LaTorraca et al. [26], Kubica [27], and Straley et al. [28] found that permeability k can be better predicted by using T_2 instead of T_1 with no significant change in the exponents, and the model was improved to $k = C\phi^4 T_{2\mathrm{LM}}^2$ (Straley et al. [28]). However, the equation was determined only from the data of sandstones (e.g., Berea and, Fontainebleau sandstones) and limestones (e.g., Portland limestones). This model is more commonly written as $k = C\phi^{m_1} T_{2\mathrm{LM}}^{n_1}$ (SDR model), and the values of 4 and 2 for m_1 and n_1 are used as empirical values. Here, C is a constant that depends on the surface relaxivity and mineralogy. $T_{2\mathrm{LM}}$ is the logarithmic mean value of the T_2 distribution. When there are two phases (oil and water) in pores with water saturation S_{w}, the permeability of the water phase k_{w} [29] can be expressed as

$$k_{\mathrm{w}} = C\phi_{\mathrm{w}}^{m_1} T_{2\mathrm{wLM}}^{n_1} \tag{5}$$

From Archie's equations ($RI = R_{\mathrm{t}}/R_{\mathrm{o}} = S_{\mathrm{w}}^{-n}$ and $F = R_{\mathrm{o}}/R_{\mathrm{w}}$), we have

$$RI = \frac{R_{\mathrm{t}}/R_{\mathrm{w}}}{R_{\mathrm{o}}/R_{\mathrm{w}}} = \frac{F_{\mathrm{w}}}{F} = S_{\mathrm{w}}^{-n} \tag{6}$$

Substitute Eq. (2) into Eq. (6), we have

$$\frac{F_{\mathrm{w}}}{F} = \left(\frac{V_{\mathrm{w}}}{V}\right)^2 \cdot \left(\frac{A}{A_{\mathrm{w}}}\right)^2 \cdot \frac{k}{k_{\mathrm{w}}} = S_{\mathrm{w}}^{-n} \tag{7}$$

Substitute Eq. (5) into Eq. (7), we have

$$\left(\frac{V_{\mathrm{w}}}{V}\right)^2 \cdot \left(\frac{A}{A_{\mathrm{w}}}\right)^2 \cdot \left(\frac{T_{2\mathrm{LM}}}{T_{2\mathrm{wLM}}}\right)^{n_1} = S_{\mathrm{w}}^{-n+m_1} \tag{8}$$

where V is the pore volume ($\mu\mathrm{m}^3$), A is the surface area of the pore interface ($\mu\mathrm{m}^2$), V_{w}, and A_{w} and $T_{2\mathrm{wLM}}$ are parameters when the pores are partially saturated with water.

When water is the wetting phase and conductive, we assumed that the pore geometry and porosity of the medium did not change during the drainage processes. (For the tight sandy conglomerate in the study, the displacement rate was extremely low, and the process could be considered quasi-static. The samples were dried after displacement and were saturated with formation water again; the T_2 spectra did not show significant changes compared to the fully saturated

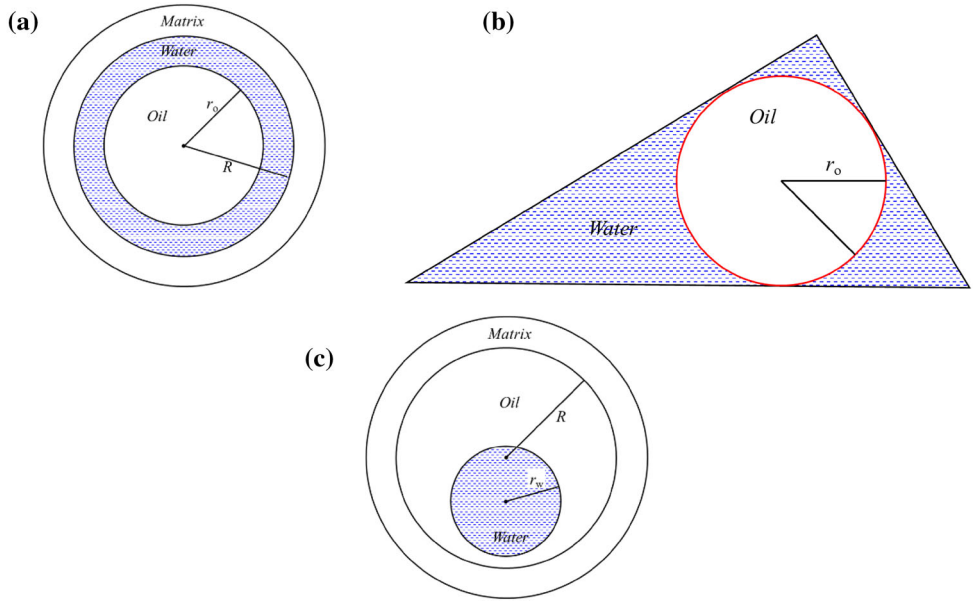

Fig. 1 Illustration of the cross sections of water and oil distribution in pores: **a** water is wetting phase; **b** water is wetting phase and the cross section of the pore-throat is a random triangle; **c** water is non-wetting phase

T_2 spectra before displacement. Therefore, this assumption was reasonable for those tight cores.). If the pore geometry is composed of uniform cylindrical pore channels and in a cross-section view, the oil–water distribution in the pores is as illustrated in Fig. 1a, and the equation can be simplified as

$$\frac{V_w}{V} = S_w = \frac{\pi(R^2 - r_o^2)l}{\pi R^2 l} = 1 - \left(\frac{r_o}{R}\right)^2 \tag{9}$$

$$\frac{A_w}{A} = \frac{2\pi(R + r_o)l}{2\pi Rl} = 1 + \frac{r_o}{R} \tag{10}$$

where R is the pore radius (μm), r_o is the equivalent oil column radius (μm), r_w is the equivalent water column radius (μm), and l is the length of the pore channel (μm). When Eqs. (8), (9), and (10) are combined, we obtain the saturation exponent n_w in a water-wet condition (here, n in Eq. (8) is replaced by n_w) of uniform cylindrical pore channels:

$$n_w = m_1 - 2 + \frac{2\ln\left[1 + (1 - S_w)^{0.5}\right] + n_1 \ln\left(\frac{T_{2wLM}}{T_{2LM}}\right)}{\ln(S_w)} \tag{11}$$

While in real reservoirs, most pores have irregular and random shapes, we assumed that the cross section of the pore geometry is a random triangle, as illustrated in Fig. 1b. When water is the wetting phase, supposing that oil is uniformly distributed in the central part of the pore geometry with a cylindrical shape having a radius r_o, we can obtain

$$\frac{V_w}{V} = S_w = \frac{(A - \pi r_o^2)l}{Al} = 1 - \frac{\pi r_o^2}{A} \tag{12}$$

$$\frac{A_w}{A} = \frac{(2\pi r_o + P)l}{Pl} = 1 + \frac{2\pi r_o}{P} \tag{13}$$

Substituting Eqs. (12) and (13) into Eq. (8), we obtain the saturation exponent n_w in a water-wet condition of an irregular cross section, which can be represented as

$$n_w = m_1 - 2 + \frac{2\ln\left[1 + \sqrt{4\pi G}(1 - S_w)^{0.5}\right] + n_1 \ln\left(\frac{T_{2wLM}}{T_{2LM}}\right)}{\ln(S_w)} \tag{14}$$

where G is the shape factor of the cross section of the pore, which is equal to the ratio of the cross-sectional area to the square of the cross-sectional circumference ($G = A/P^2$), A is the area of the triangle (μm^2), and P is the circumference of the triangle (μm).

For water in the non-wet phase in Fig. 1c, the saturation exponent is deduced in "Appendix."

3 Materials and Methods

3.1 Rock Samples

To validate the proposed models in the paper, 21 sandy conglomerate cylindrical rock core samples approximately 8 cm

in length from three districts (M, X, F) of the Junggar Basin, Northwestern China, were selected. The porosity ranges from 4.0 to 12.2%, with an average of 8.7%; the permeability ranges from 0.006 to 0.746 mD, with an average of 0.147 mD.

3.2 Experimental Process

The cores were cut into three parts and the first part, approximately 5 cm in length, was used for rock resistivity and NMR experiments. The second part, approximately 2 cm in length, was used for high-pressure mercury injection. The last part was used for SEM and thin section analysis. Samples were carefully cleaned of washing oil by methylbenzene and then were dried at 105 °C for 48 h. The helium porosity and nitrogen permeability were obtained by a Core Lab CMSTM-300 automated permeameter at a confining pressure of 3.0 MPa. Then, cores were saturated with 15,000 ppm NaCl by immersion under vacuum (more than 48 h at 20 MPa) to ensure that the brine fully saturated the pore spaces. Low field nuclear magnetic resonance equipment (RecCore2500, China) was used for the T_2 spectra measurement. The CPMG (Carr–Purcell–Meiboom–Gill) sequence was selected, and the waiting time (T_W), echo time (T_E), echo number (NECH) and scanning number were set to 6000 ms, 0.301 ms, 18,000 and 32, respectively. The T_2 spectra of the fully water-saturated core samples were measured. The samples were loaded into an electric core holder, and the electrical resistivity was measured under a confining pressure of 7.0 MPa by using a high-temperature and high-pressure multi-parameter testing unit (SCMS-E, China) following the Chinese Oil and Gas Industry Standard (SY/T 5385-2007); the professional equipment has two electrodes, and the cores were maintained for at least 2 h to ensure that the unit output stable data. Then, cores were displaced by nitrogen gas under a displacement pressure of 5.0 MPa until no water was discharged. The electrical resistivity under this partial water-saturated condition was measured again, and then, the T_2 spectra were also obtained at the same parameter settings for the fully water-saturated condition. The high-pressure injected mercury analysis was performed on the Micrometrics Auto pore IV 9520 mercury apparatus following the standard SY/T 5346-2005 of China. The maximum injection pressure was 200 MPa, corresponding to a pore-throat size of 0.0036 μm.

4 Results and Discussion

Water saturation is greatly affected by wettability in the porous media. Therefore, the proposed saturation exponent models were distinguished into oil- or water-wet in our study (Eq. (14) for water-wet and Eq. (A7) for oil wet). During the experiment, the samples were carefully cleaned with methylbenzene to cut oil, and then, two samples were selected to measure the wettability by using the Amott method [30] (Neutral wetting kerosene and 15,000 ppm NaCl were used as the simulation fluid). The results showed that a large amount of oil was driven out during the water imbibition process (Fig. 2a), while no water was driven out during the oil imbibition process (Fig. 2b). The Amott indexes were calculated and equal 0.736 and 0.704, we can conclude that the samples were obviously water wet.

The pores are identified by thin section and SEM images in Fig. 3 and are classified into four types: original intergranular pores, residual intergranular pores, grain dissolution pores,

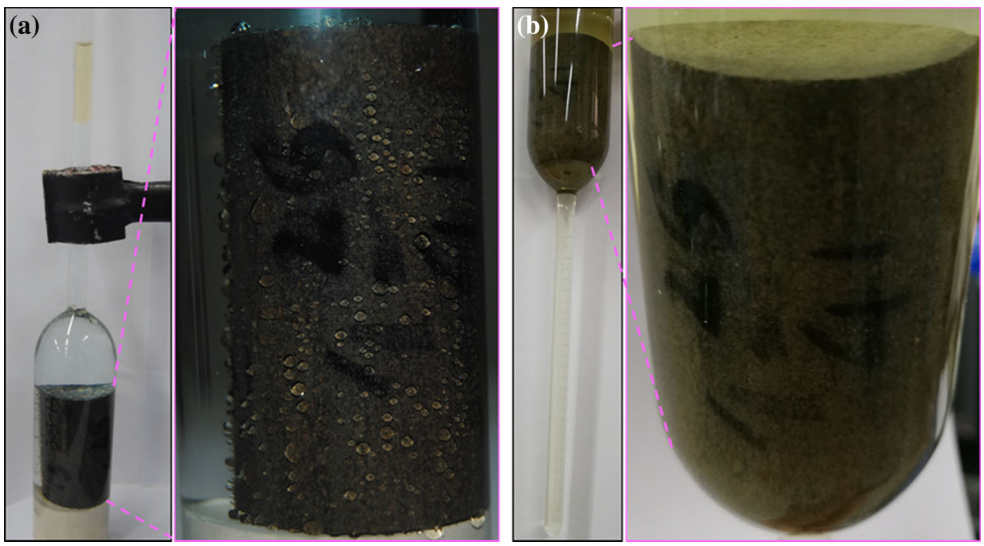

Fig. 2 **a** Oil droplets at the surface of the cylindrical core plug during spontaneous imbibition experiment in water; **b** core plug spontaneous imbibition in oil

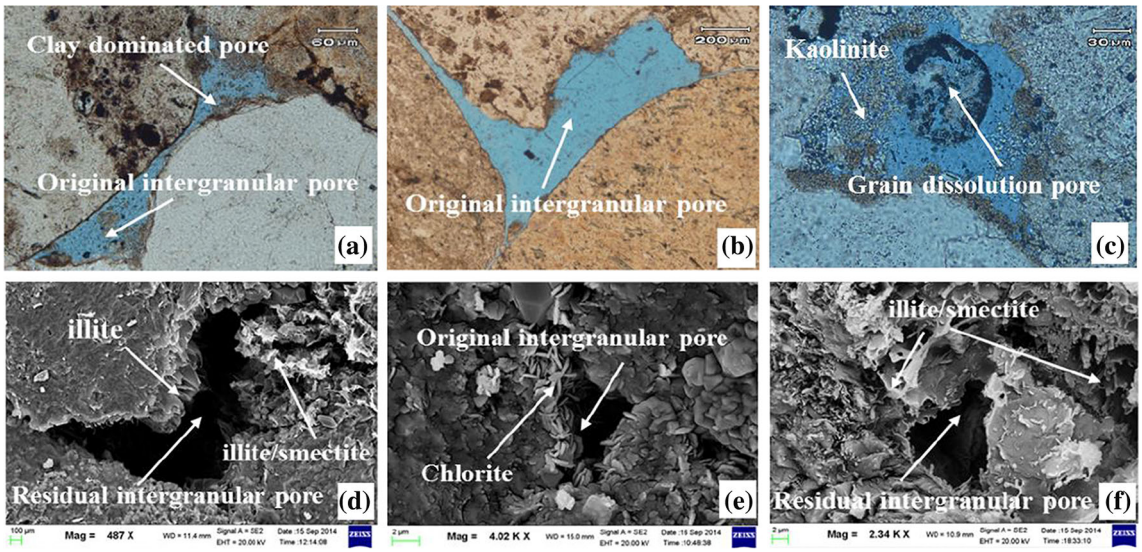

Fig. 3 SEM images of rock fragment surfaces and transmitted light images of thin sections of rock impregnated with blue epoxy. **a** FN10-7, **b** M133-2, **c** 152-15, **d** M133, depth: 3301.57 m, **e** M134, depth: 3174.58 m, **f** M133, depth: 3366.98 m

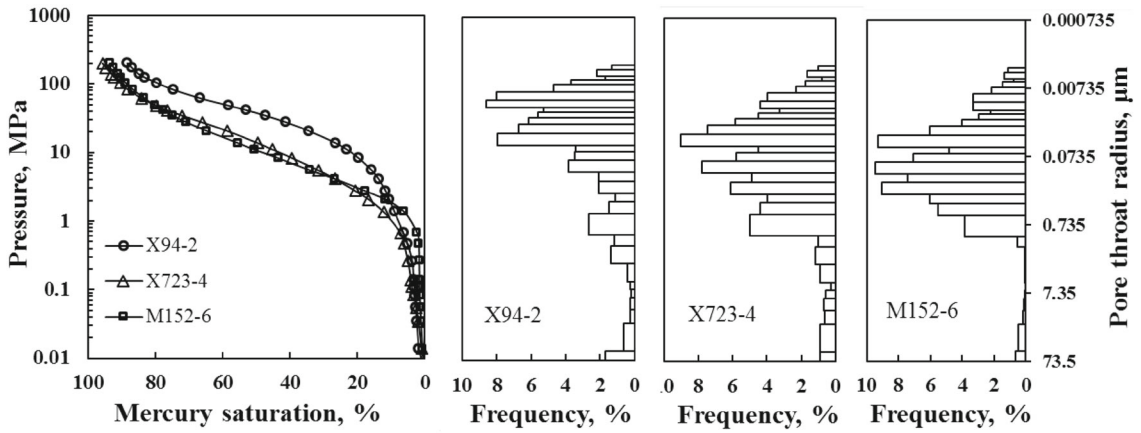

Fig. 4 Intrusion curves of pressure-controlled porosimetry and corresponding pore-throat size distribution for three samples

and clay-dominated pores. Original intergranular pores and residual intergranular pores are the main types, and the pore shapes are triangle or irregular polygon. The intrusion curves from the pressure-controlled porosimetry of three samples (X94-2, X723-4, M152-6) show no horizontal stage, with the mercury injection pressure increasing from the beginning to the end (Fig. 4). The overall pore-throat size varies from 0.012 to 1.094 μm based on the equation $r_c = 0.735/p_c$ [31], which indicates a typical microsize. The average threshold pressure is 0.674 MPa, which corresponds to the average maximum pore-throat radius of 1.091 μm. The medium-saturation pressure shows little difference and ranges from 10.750 to 37.713 MPa, which corresponds to the medium radius ranges from 0.068 to 0.019 μm. Figure 5 displays the NMR T_2 spectra of the samples fully saturated with water. The majority of the spectra is located in the range of $T_2 < 10$ ms, which is typically associated with micropores. Though the shape of the T_2 spectra changes significantly with pore geometry and mineralogy, the NMR porosity values do not vary significantly with lithology or salinity, so the volume of water can be calculated. The fully and partially water-saturated T_2 spectra for three samples are shown in Fig. 6. We can find that the T_2 spectra after nitrogen displacement shows a bimodal characteristic and that the T_2 times are mainly distributed in the range of less than 10 ms, which corresponds to the dominant bound water.

The first point to be discussed here is the appropriateness of Eq. (2) for tight sandy conglomerate reservoirs. Based on the thin section and SEM images in Fig. 3, tight sandy conglomerate cores could be equivalent to those composed of pore-throat channels. Meanwhile, the co-relationships between $\log F$ and $\log k$ for 21 samples are plotted in Fig. 7 and fitted for different districts (M, X, F), which showed good correlation. Thus Eq. (2) is used directly in this tight sandy

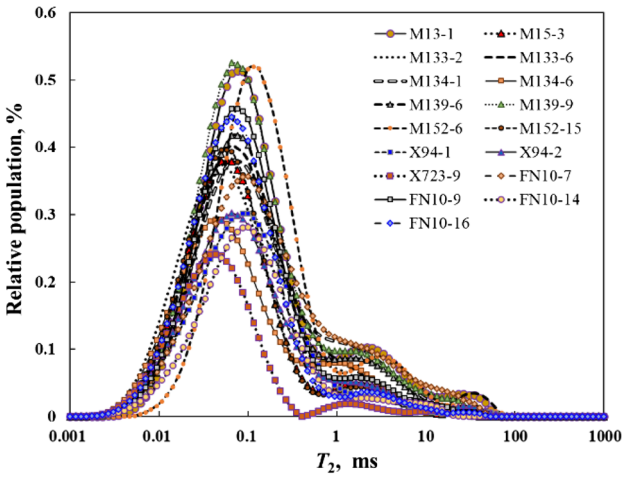

Fig. 5 The NMR T_2 spectra of the 21 fully water-saturated rock samples

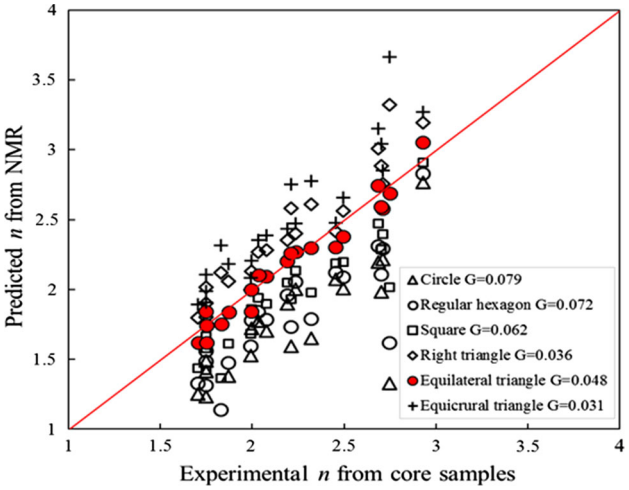

Fig. 8 Comparison between predicted and measured values of saturation exponent n for six different pore geometry

conglomerate reservoir. For the effect of pore geometry on the saturation exponent n, we introduced the shape factor G, which is obtained from thin sections and SEM images based on statistical analysis. In our study, two thin sections and 10 SEM images were obtained for one sample, which was sufficient to indicate the pore-throat geometry. The thin sections and SEM images in Fig. 3 exhibit that the geometric shape of the pores is irregular, and triangle is the main type. Seven pore geometries (circle, regular hexagon, square, right triangle, equilateral triangle, and equicrural triangle) were also chosen to interpret the relationship between G and n. The results demonstrate that the measured and predicted n have good agreement when the pores are equivalent to an equilateral triangle (Fig. 8). That is, $G = 0.048$ is an appropriate value for the tight sandy conglomerate reservoir. Meanwhile, the difference of the exponent n between considering pore geometry and not considering pore geometry is also plotted in Fig. 9. It appears that n is more optimized with G compared to the experimental data.

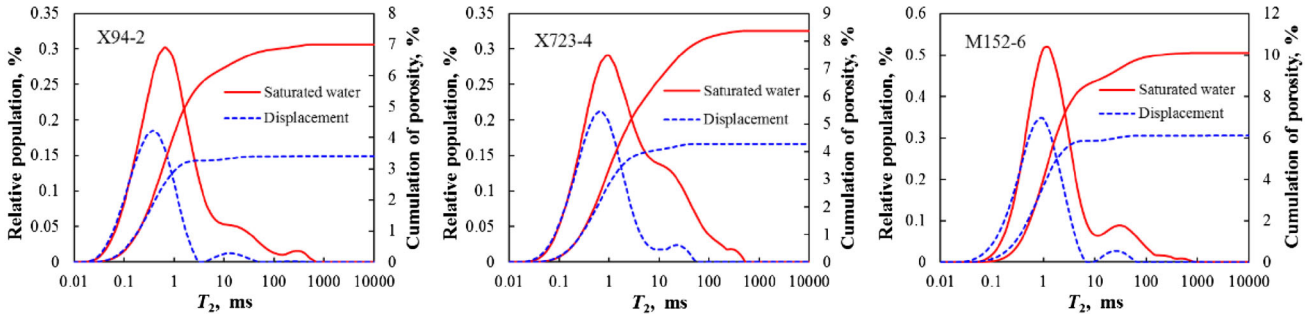

Fig. 6 The NMR T_2 spectra under different water saturation conditions for three samples

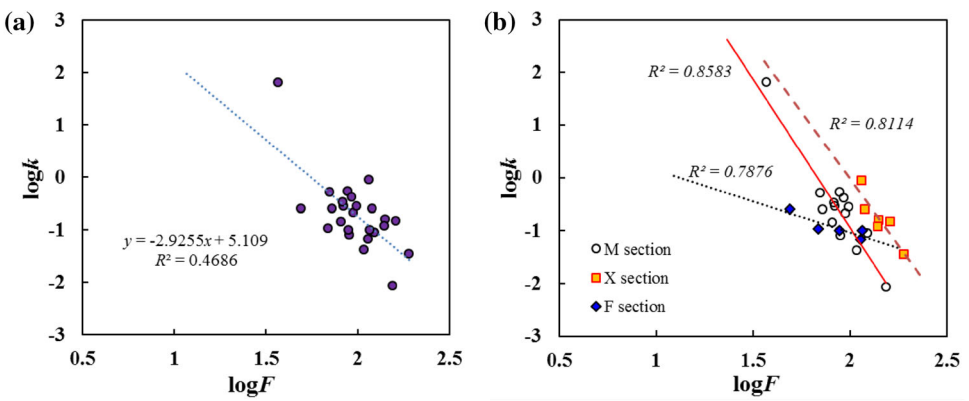

Fig. 7 Correlation between log$F$ and log$k$ for 21 samples

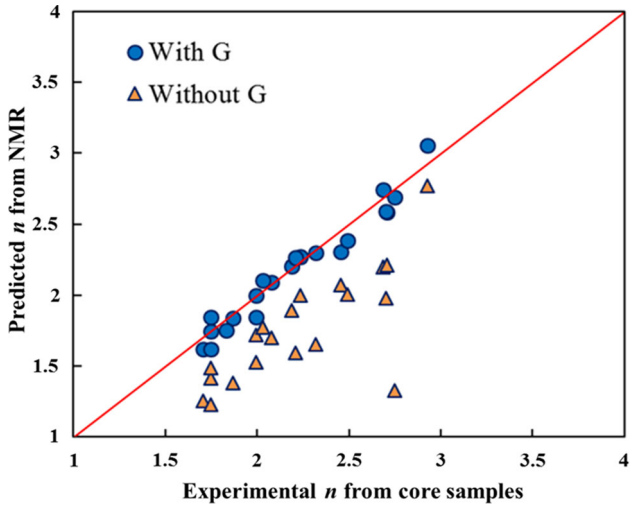

Fig. 9 Comparison between predicted n with or without G and the measured n $\left(n_{\text{measured}} = -\frac{\lg(R_t/R_o)}{\lg S_w}\right)$

The values of the coefficients C, m_1 and n_1 were determined by multiple regression analysis based on the SDR model. As the samples were selected from three districts in the Junggar Basin, the relationships between the porosity and permeability are not the same, and the values of m_1 and n_1 are different for the three districts, e.g., m_1 equals 4.504, 4.704 and 4.704 and n_1 equals 0.685, 1.012 and 1.385 for districts M, X and F, respectively.

The difference between the saturation exponent from our model (Y-axis) and the saturation exponent from Archie's Law (X-axis) was compared and is plotted in Fig. 10a. The water saturation predicted by our model (Y-axis) was also compared with the measured water saturation by weight (X-axis) in Fig. 10b to validate our model. The predicted values of n lie in the range of 1.618–3.055, and the measured values of n (calculated by $n = \lg(R_o/R_t)/\lg S_w$ based on experimental data) have a distribution between 1.703 and 2.927 (Fig. 10a). The two dashed lines show the absolute error between the predicted and measured values, which is −0.153 to 0.131. According to the saturation exponent model (Eq. (14)), the water saturation of the partially saturated tight sandy conglomerate reservoir can be predicted. The comparison results of the predicted and measured values of the water saturation (Table 1) are plotted in Fig. 10b. We find that the predicted values of S_w vary in the range of 41–93%, the measured values range from 38–93% (Fig. 10b) and the absolute error of the two saturation values from −0.032 to 0.023. These results show that the new model has good adaptability to tight sandy conglomerate reservoirs.

5 Conclusion

(1) Taking advantage of the NMR method in the core analysis and saturation evaluation of reservoir fluids, this research developed the conventional Archie equation based on the SDR model. The shape factor G was introduced to characterize the irregularity of the pores cross section, and we derived a model for calculating the saturation exponent n under different fluid contribution condition. According to the model, the saturation exponent n is a function of the pore geometry and water saturation and possesses clear variances under a water-wet condition.

(2) The proposed model aims to calculate the water saturation of tight sandy conglomerate reservoirs under water-wet conditions. When the pores are equivalent to an equilateral triangle, the value of G is appropriate for real reservoirs. The improved model has an obvious advantage in calculating the water saturation, and the predicted values obtained by the model under water-wet condition have good agreement with the experimental data from tight sandy conglomerate reservoirs.

(3) In tight reservoirs, the wetting phase is a thin membrane, and the non-wetting phase forms an irregular shape when

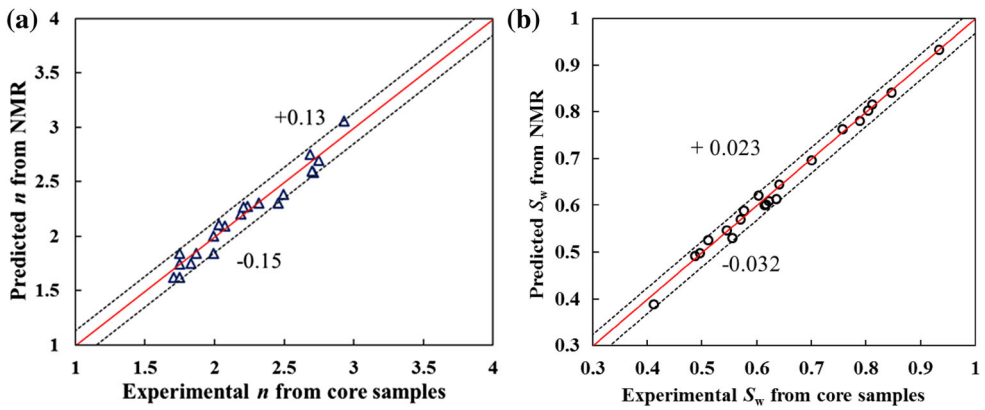

Fig. 10 **a** Comparison between the predicted and the measured values of the saturation exponent n; **b** Comparison between the predicted and the measured values of the water saturation S_w

Table 1 Summary of the 21 samples selected in this study

Sample	$S_w(f)$	R_o (Ω m)	R_w (Ω m)	R_t (Ω m)	T_{2LM}	T_{2wlm}	n Measured	$m1$	$n1$	n Predicted	S_wPredicted (f)
M13-1	0.556	30.552	0.478	98.413	1.473	0.500	1.993	4.004	0.685	1.843	0.530
M15-3	0.545	39.828	0.478	150.391	0.770	0.365	2.189	4.504	0.885	2.205	0.547
M133-2	0.642	55.015	0.592	138.187	0.739	0.383	2.076	4.504	0.885	2.093	0.644
M133-6	0.701	77.275	0.478	150.333	1.161	0.582	1.871	4.504	0.685	1.840	0.696
M134-1	0.412	55.982	0.592	495.025	1.379	0.457	2.455	4.504	0.685	2.303	0.388
M134-6	0.571	75.299	0.592	200.598	0.840	0.368	1.749	4.204	0.685	1.743	0.570
M139-6	0.617	58.091	0.592	132.334	1.266	0.607	1.704	4.204	0.685	1.620	0.602
M139-9	0.637	38.827	0.592	85.514	1.248	0.599	1.750	4.204	0.685	1.617	0.614
M152-3	0.622	39.413	0.478	128.714	1.872	0.748	2.494	4.704	0.685	2.381	0.608
M152-6	0.604	42.874	0.478	103.431	1.899	0.861	1.747	4.504	0.585	1.843	0.620
M152-15	0.758	51.023	0.592	107.506	0.718	0.457	2.684	4.504	1.585	2.746	0.762
M154-6	0.497	42.935	0.592	173.224	3.373	1.156	1.994	4.204	0.685	1.998	0.497
X90-1	0.615	61.082	0.592	227.674	1.719	0.652	2.709	4.204	1.000	2.580	0.601
X723-9	0.934	91.249	0.592	110.155	0.496	0.414	2.748	4.704	2.000	2.689	0.932
X723-4	0.512	67.968	0.592	482.605	2.169	0.721	2.928	4.704	1.000	3.054	0.526
X94-1	0.847	90.927	0.478	123.236	1.041	0.741	1.832	4.904	1.000	1.750	0.840
X94-2	0.487	67.226	0.478	335.891	1.048	0.393	2.237	4.704	0.585	2.271	0.492
FN10-7	0.577	52.597	0.592	160.860	1.814	0.651	2.033	4.504	0.585	2.105	0.588
FN10-9	0.789	40.809	0.592	77.472	1.024	0.671	2.702	4.704	1.385	2.593	0.781
FN10-14	0.812	67.254	0.592	106.596	1.104	0.776	2.210	4.704	1.385	2.261	0.816
FN10-16	0.804	29.106	0.592	48.260	0.788	0.548	2.319	4.704	1.385	2.300	0.803

Measured water saturation after displacement S_w, resistivity of the fully saturated rock R_o, resistivity of the pore fluid R_w, resistivity of the partly saturated rock R_t, the logarithmic mean of transversal relaxation time T_{2LM}, measured saturation exponent (n, measured), predicted saturation exponent (n, predicted), coefficients of SDR model (m_1, n_1), and predicted water saturation (S_w, predicted)

the saturation of non-wetting phase is high. For partly water-saturated samples, calculating the saturation exponent was difficult, as the relative permeability was not measured for these samples. Eq. (5) is not validated based on the experimental data at this point, and we intend to finish this validation during our next work.

Acknowledgements This project was supported by the National Natural Science Foundation of China (No. 41504108).

Appendix

When water in the pores is the non-wetting phase, the oil phase adheres to the surface of the solid grains of the rock, forming an oil membrane. In this case water is distributed in the center part of the pore geometry, as shown in Fig. 1c. Accordingly Eqs. (9) and (10) change into

$$\frac{V_w}{V} = S_w = \frac{\pi r_w^2 l}{\pi R^2 l} = \left(\frac{r_w}{R}\right)^2 \tag{A1}$$

$$\frac{A_w}{A} = \frac{2\pi r_w l}{2\pi R l} = \frac{r_w}{R} \tag{A2}$$

Combining Eqs. (A1) and (A2) with Eq. (8), we obtain

$$S_w^{n+1} = \frac{k_w}{k} = S_w^{m_1}\left(\frac{T_{2wLM}}{T_{2LM}}\right)^{n_1} \tag{A3}$$

Therefore, the saturation exponent n in the oil-wetting condition is:

$$n_{nw} = m_1 - 1 + n_1 \frac{\ln\left(\frac{T_{2wLM}}{T_{2LM}}\right)}{\ln(S_w)} \tag{A4}$$

Equations (11) and (A4) are the saturation exponent models under different wetting conditions when the pores have a regular shape.

When the cross section of the pore geometry is a triangle, as illustrated in Fig. 1b, and water is in the wetting phase, supposing that the oil phase is uniformly distributed in the central part of the pore geometry with a cylindrical shape having a radius r_o, we can obtain

$$\frac{V_w}{V} = S_w = \frac{(A - \pi r_o^2)l}{Al} = 1 - \frac{\pi r_o^2}{A} \tag{A5}$$

$$\frac{A_w}{A} = \frac{(2\pi r_o + P)l}{Pl} = 1 + \frac{2\pi r_o}{P} \tag{A6}$$

Substituting Eqs. (A5) and (A6) into Eq. (8), we can obtain the saturation exponent n when oil is the wetting phase:

$$n_{nw} = m_1 - 1 + \frac{\ln(4\pi^2 G) + n_1 \ln\left(\frac{T_{2\mathrm{wLM}}}{T_{2\mathrm{LM}}}\right)}{\ln(S_{\mathrm{w}})} \tag{A7}$$

References

1. Archie, G.E.: The electrical resistivity log as an aid in determining some reservoir characteristics. Trans. AIME **146**, 54–61 (1942)
2. Alkafeef, S.F.; Alajmi, A.F.: The electrical conductivity and surface conduction of consolidated rock cores. J. Colloid Interface Sci. **309**, 253–261 (2007)
3. Tabbagh, A.; Cosenza, P.: Effect of microstructure on the electrical conductivity of clay-rich systems. Phys. Chem. Earth Parts A B C **32**, 154–160 (2007)
4. Kumar, M.; Senden, T.J.; Sheppard, A.P.; Arns, C.H.; Knackstedt, M.A.: Probing the Archie's exponent under variable saturation conditions. Petrophysics **52**, 124–134 (2011)
5. Clavier, C.; Coates, G.; Dumanoir, J.: Theory and experimental basis for the dual-water model for interpretation of shaly sands. SPE (1977)
6. Xiao, L.; Zou, C.C.; Mao, Z.Q.; Shi, Y.J.; Liu, X.P.; Jin, Y.; Guo, H.P.; Hu, X.X.: Estimation of water saturation from nuclear magnetic resonance (NMR) and conventional logs in low permeability sandstone reservoirs. J. Pet. Sci. Eng. **108**, 40–51 (2013)
7. Haro, C.F.: Permeability modeling. Setting Archie and Carman–Kozeny Right. In: SPE Europec/EAGE Annual Conference and Exhibition (2006)
8. Haro, C.F.: The equations archie forgot: anisotropy of the rocks. SPE Reserv. Eval. Eng. **13**, 823–836 (2010)
9. Knight, R.; Endres, A.: An introduction to rock physics principles for near-surface geophysics. SEG Investig. Geophys. **13**, 31–70 (2005)
10. Yue, W.Z.; Tao, G.: A new non-Archie model for pore structure: numerical experiments using digital rock models. Geophys. J. Int. **195**, 282–291 (2013)
11. Rasmus, J.C.: Summary of the effects of various pore geometries and their wettability on measured and in-situ values of cementation and saturation exponents. Log Anal. **28**, 152–164 (1987)
12. Berg, C.R.: Effective-medium resistivity models for calculation water saturation in shaly sands. Log Anal. **37**, 16–28 (1996)
13. Montaron, B.: Connectivity theory—a new approach to modeling non-Archie rocks. Petrophysics **50**, 102–115 (2009)
14. Suman, R.J.; Knight, R.J.: Effects of pore structure and wettability on the electrical resistivity of partially saturated rocks-a network study. Geophysics **62**, 1151–1162 (1997)
15. Man, H.N.; Jing, X.D.: Network modelling of mixed-wettability on electrical resistivity, capillary pressure and wettability indices. J. Pet. Sci. Eng. **33**, 101–122 (2002)
16. Simandoux, P.: Dielectric measurements on porous media, application to the measurement of water saturations, study of the behavior of argillaceous formations (translated by L. Moinard, in the SPWLA Shaly sand reprint volume, 1982). Revue de l'Institut Francais du Petrole, pp. 193–215 (1963)
17. Poupon, A.; Leveaux, J.: Evaluation of water saturation in shaly formations. In: Transactions, SPWLA 12th Annual Logging Symposium, paper O (1971)
18. Waxman, M.H.; Thomas, E.C.: Electrical conductivities in shaly sands-I. The relation between hydrocarbon saturation and resistivity index; II. The temperature coefficient of electrical conductivity. SPE J. **12**, 213–225 (1974)
19. Clavier, C.; Coates, G.; Dumanoir, J.: Theoretical and experimental bases for the dual-water model for interpretation of shaly sands. SPE J. **24**, 153–168 (1984)
20. Juhasz, I.: Normalized Qv—the key to shaly sand evaluation using the Waxman–Smits equation in the absence of core data. In: Transactions, SPWLA 22nd Annual Logging Symposium, 23–26 June, paper Z (1981)
21. Anderson, W.G.: Wettability literature survey. Part 3: The effects of wettability on the electrical properties of porous media. J. Pet. Technol. **39**, 1371–1378 (1986)
22. Walsh, J.B.; Brace, W.F.: The effect of pressure on porosity and the transport properties of rock. J. Geophys. Res. Atmos. **89**, 9425–9432 (1984)
23. Jorand, R.; Fehr, A.; Koch, A.; Clauser, C.: Study of the variation of thermal conductivity with water saturation using nuclear magnetic resonance. J. Geophys. Res. Atmos. **116**, 4684–4698 (2011)
24. Seevers, D.O.: A nuclear magnetic method for determining the permeability of sandstones. In: Transactions, SPWLA 6, paper L (1966)
25. Kenyon, W.E.: Nuclear magnetic resonance as a petro physical measurement. Nucl. Geophys. **6**, 153–171 (1992)
26. LaTorraca, G.A.; Dunn, K.J.; Brown, R.J.S.: Predicting permeability from nuclear magnetic resonance and electrical properties measurement. In: Society of Core Analysts Conference, SCA-9312, Sept 1993 (1993)
27. Kubica, P.: Statistical test of permeability estimates based on NMR measurements. In: Transactions, SPWLA 36, paper VVV (1995)
28. Straley, C.; Rossini, D.; Vinegar, H.J.; Tutunjian, P.; Morriss, C.E.: Core analysis by low-field NMR. Log Anal. **38**, 84–93 (1997)
29. Alghamdi, T.M.; Arns, C.H.: Predicting relative permeability from NMR relaxation-diffusion responses utilizing high resolution micro X-ray-CT images. SPE (2012)
30. Amott E.; Aime M.: Observations relating to the wettability of porous rock. SPE, pp. 156–162 (1959)
31. Schmitt, M.; Fernandes, C.P.; Neto, J.A.B.D.C.; Wolf, F.G.; Santos, V.S.S.D.: Characterization of pore systems in seal rocks using nitrogen gas adsorption combined with mercury injection capillary pressure techniques. Mar. Pet. Geol. **39**, 138–149 (2013)